Semi-analytical Modelling of 3D Fully-Dielectric Metamaterials

Miguel A. Balmaseda-Márquez*, Guido Valerio†‡, Carlos Molero Jiménez*,
Ángel Palomares-Caballero*, Pablo Padilla*
*Department of Signal Theory, Telematics and Communications, Universidad de Granada (CITIC-UGR),
18071 Granada, Spain,
migbalmar@ugr.es, cmoleroj@ugr.es, angelpc@ugr.es, pablopadilla@ugr.es
†Sorbonne Université, CNRS, Laboratoire de Génie Electrique et Electronique de Paris (GeePs), 75252, Paris, France,
guido.valerio@sorbonne-universite.fr
‡Université Paris-Saclay, CentraleSupélec, CNRS, GeePs, 91192, Gif-sur-Yvette, France

***Abstract*—This paper presents a novel type of characterization for 3D fully-dielectric unit cell. The unit cell structure is formed by a block of dielectric with different inserts of air on it. The performed characterization is carried out up to the frequency where the electric-size of the unit cell is $\lambda/2$. Based on the results obtained in simulation, design equations for the effective permittivity can be extracted for the two different dielectric unit cell designs. Using equivalent circuit, several arrangements of dielectric unit cells have been modelled. The results obtained with the circuit models are in good agreement with the simulated S parameters in a wide frequency range.**

***Index Terms*—Circuit model, design equations, dielectric, metamaterial, unit cells.**

I. Introduction

Fully-dielectric passive terminals have emerged as a interesting alternative for applications in the millimeter range to design high-gain antennas. Furthermore, the evolution of 3D printing technology has enabled a great tool to bring to reality fully-dielectric antennas that were very costly to manufacture with conventional methods in the past. Among the different types of antennas that can be made with only dielectrics, we can highlight dielectric resonator antennas (DRA) [1], [2], reflectarrays (RA) [3], [4], transmitarrays (TA) [5], [6] and lenses [7]–[20].

Depending on the type of antenna to be considered, a single or a certain range of permittivity values are generally required for a successful design. For instance, depending on the desired type of lens antenna, a refractive index map (or permittivity map if only dielectric material is used) must be considered. This fact leads to planar (or semi-planar) panels with permittivity gradients (ε_r varying in space) to be implemented in the design and manufacturing process [9]. A widely used way to achieve the range of permittivities needed for a determined fully-dielectric antenna design is to use a unit cell composed of dielectric and air. In this manner, the ratio between the space covered by air versus that occupied by dielectric in the cell allows for the control of the effective ε_r of the cell from 1 (entire space filled with air) to the permittivity of the dielectric being used (entire space filled with the dielectric). Many papers in the literature use this technique to synthesize the ε_r range needed by the unit cells of their antenna design [9], [11], [12], [16], [18]. Moreover, based on the effective medium theory, some of the reported works approximate the resulting ε_r of the unit cell as volumetric average of the air and the remaining dielectric material [21]. However, this is valid as long as the unit cell analyzed is electrically quite small with respect to the wavelength in the homogenized ε_r [20]. Otherwise this approach is not valid.

In this paper, two different dielectric unit cell designs are analyzed beyond the range of validity of the effective medium theory (unit cell electrical-sizes up to half of the wavelength ($\lambda/2$) in the homogenized dielectric). For this purpose, the percentage of dielectric in the unit cells is varied up to a complete filling. Additionally, thanks to the characterization of the homogenized ε_r of the dielectric unit cells, a circuit model has been developed that allows for an efficient evaluation of the phase and magnitude of several concatenated dielectric unit cells. The models are told to be semi-analytical due to the fact that numerical simulations are needed to extract valuable information. However, physical arguments are applied to obtain the value of the parameters.

This work is organized as follows. In Section II, the dielectric unit cell designs and their characterization are presented. Analytical equations to parameterize circuit-model elements are deduced from the simulations and explained in the section. In Section III, some comparison between the derived circuit models and different arrangements of dielectric unit cells are performed. Finally, the conclusions are detailed in Section IV.

II. Unit Cell Definition and Characterization

The unit cells are formed by a volumetric dielectric material of permittivity ε_{r} inserted in an air square box of periodicity d. The cross section of the cell is uniform along the propagation direction (z-axis), whose length is parametrized by l. Fig. 1(a) shows a perspective view of the T-shaped cell. Periodic boundary conditions are enforced along the x and y directions, and a propagation along the z axis is assumed. In this work, two different unit-cell cross sections are considered: squared-

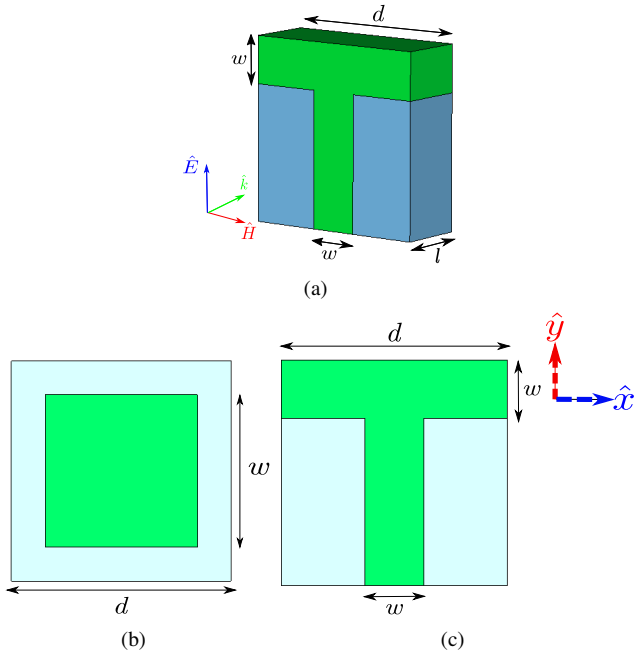

Fig. 1. (a) Perspective view of the T-shaped unit cell, d_1 is fixed to 1mm in all cases. Cross section of the unit cell: (a) Square-shaped unit cell (b) T-shaped unit cell. Blue and green zones correspond to air and dielectric, respectively.

and T-shaped, as shown in Fig. 1(b) and 1(c), respectively. Both geometries are controlled by a single parameter w. The cell is illuminated by a plane wave, impinging normally and having a vertically-polarized electric field (along the y direction according to the frame of coordinates in Fig. 1(a)). We will study how these unit cells behave when the proportion dielectric volume/cell volume (filling factor, χ) is modified. This is achieved by modifying w while keeping d fixed in both cases ($d = 2.7\,\text{mm}$). The length of each unit cell is fixed to be $l = 1\,\text{mm}$.

For the sake of performing a comprehensive study, different permittivity values of the dielectric material are studied, in particular, $\varepsilon_\text{r} = [2.6, 5, 8]$. For each of these cases, parametric studies have been carried out, consisting of the evaluation of the scattering parameters of the unit cell with respect to the filling factor χ. This allows us to compute the effective permittivity of the unit cell $\varepsilon_{\text{r, eff}}$.

The study is realized for different frequencies. The highest frequency considered in each of the cases is such that the wavelength approximately takes $d = \lambda/2$. In Table I, the highest frequency value of each permittivity case is displayed.

TABLE I
FREQUENCY SPANS TO STUDY DEPENDING ON THE RELATIVE PERMITTIVITY

ε_r	**Highest frequency (GHz)**
2.6	35
5.0	25
8.0	20

A. *Extraction of the effective-permittivity value*

In order to calculate the effective permittivity for each filling factor, we compute the propagation constant β of the fundamental mode inside the unit cell. The frequency values in Table I ensure the non-excitation of higher order modes. Two different ways are used to obtain the β. On the one hand, the unit cell is circuitally interpreted as the equivalent circuit in Fig 2, where Z_0 is the characteristic impedance associated with the impinging (and outgoing) plane wave, and Z is the characteristic impedance related to the mode propagating along the unit cell. The calculation of β is done by configuring and simulating a particular geometry of the unit cell. After inspecting the scattering (S) parameters of the unit cell (S_{11} and S_{21}), the propagation constant is computed just by solving the equivalent circuit via ABCD matrix formalism [22], where β is the unknown. On the other hand, a second method validating the analysis consists of the use CST eigensolver. It provides the modal solutions supported by the unit cell and their phase constants. This is a more direct method, where no additional calculations are needed.

As an example, Fig. 3 shows the evolution of β versus frequency achieved by both models in a specific geometry. For this case, a unit cell with square-shaped geometry, $\chi = 0.8$ (80% of filling) and $\varepsilon_\text{r} = 5$ has been chosen. We can appreciate the excellent agreement between both models. In fact, it is worth remarking the linearity of the evolution of β along the whole frequency range. This indicates that the effective refractive index ($n_{\text{r,eff}} = \sqrt{\varepsilon_{\text{r, eff}}}$) is constant in the frequency range.

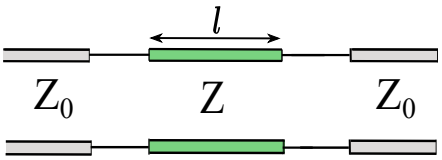

Fig. 2. Circuit model for the dielectric unit cell with length l

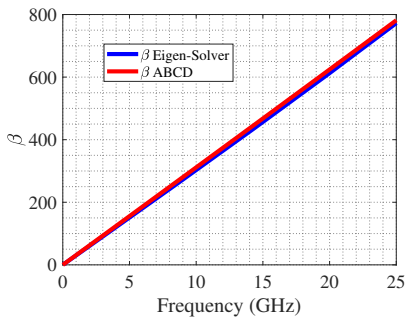

Fig. 3. Comparison between ABCD method and eigensolver for the square-shaped dielectric unit cell with a filling factor of 80% and a permittivity of 5.

Once β is computed, we can extract the effective permittivity $\varepsilon_{\text{r,eff}}$ for a single frequency point (thanks to the linear

relation) as

$$\varepsilon_{\text{r, eff}} = \left[\frac{\beta c}{2\pi f}\right]^2 \tag{1}$$

and the characteristic impedance

$$Z = \frac{120\pi}{\sqrt{\varepsilon_{\text{r,eff}}}}\,. \tag{2}$$

B. Development of the semi-analytical models

Here, we compute the effective permittivities as explained in the previous subsection, for all above unit cell configurations. Since the filling factor will be varied from $\chi = 0$ (only air) to $\chi = 1$ (only dielectric), a range of effective permittivities will be calculated for both types of cross-sectional geometries.

Fig. 4 shows the evolution of $\varepsilon_{\text{r,eff}}$ versus the filling factor χ for the square-cross section case. As expected, $\chi = 0$ gives $\varepsilon_{\text{r,eff}} = 1$, while $\varepsilon_{\text{r,eff}} = \varepsilon_{\text{r}}$ when $\chi = 1$. The other points are comprised between both extreme values, following an exponential trend (best fitting curve numerically obtained in Matlab, with $r^2 = 0.991$). This allows us to find an semi-analytical function for this case. After some mathematical manipulations, it can be demonstrated that the effective permittivity can be expressed as:

$$\varepsilon_{\text{r,eff}}(\varepsilon_{\text{r}}, \chi) = e^{\chi \log \varepsilon_{\text{r}}}\,. \tag{3}$$

Fig. 4 illustrates the curve represented by (3) in dotted lines. The fitting with the numerical points is quite good. A different permittivity calculation has been applied in [7], where a linear proportion between the dielectric constant and the filling factor is used. However this modelling demands an electrical length of the unit cell much smaller than the operation wavelength. Our model has been proven to be efficient up to, at least, $d = \lambda/2$.

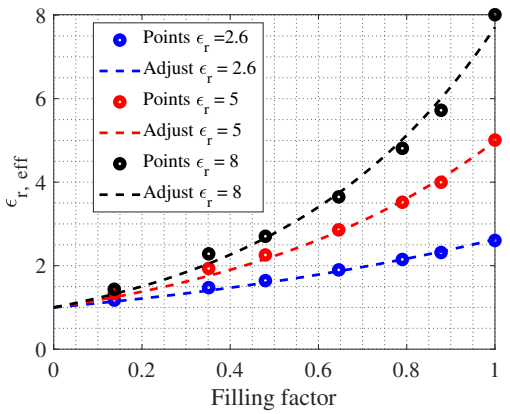

Fig. 4. Representation of the square-shaped unit cell model with the simulation performed

In the case of the T-shaped unit cell, the evolution of $\varepsilon_{\text{r,eff}}$ with respect the filling factor is exhibited in Fig. 5. Now, they seems to follows an evolution typical of potential functions (fitting curve in Matlab with $r^2 = 0.998$). A proper semi-analytical formula for this case is the following one:

$$\varepsilon_{\text{r,eff}}(\varepsilon_{\text{r}}, \chi) = (\varepsilon_{\text{r}} - 1) \cdot \chi^{1{,}289} + 1 \tag{4}$$

where b represents the growth rate of the function

$$b = 1{,}289 = \frac{\log\left(\dfrac{\varepsilon_{\text{eff},i} - 1}{\varepsilon_{\text{r}} - 1}\right)}{\log\left(\chi_i\right)}\,. \tag{5}$$

It can be demonstrated that $b = 1.289$ is satisfied for each couple of points $(\varepsilon_{\text{eff},i}, \chi_i)$ for a given ε_{r}. The curves associated to (4) fit well with the points, as shown in Fig. 5.

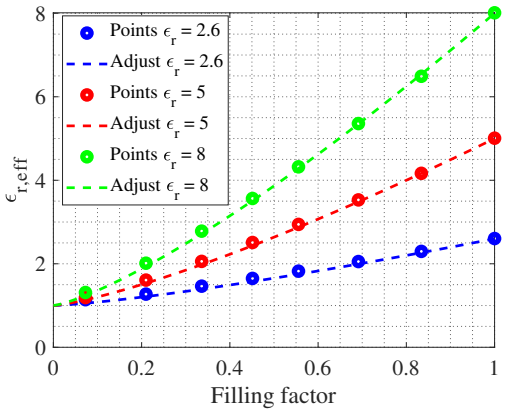

Fig. 5. Representation of the T shape model with the simulation performed

The derivation of these semi-analytical formulas is very useful, especially to be employed as design equations in fully-dielectric lenses/reflectarray/transmitarray designs. To validate them, some applications examples will be exposed in next section.

III. Applications

In order to verify the robustness of the method with arbitrarily chosen filling factors, we arrange together consecutive unit cells, and calculate the effective permittivity of the cascade. The simulations were performed using two T-shaped unit cells with the same dielectric material (ε_r = 2.6) and filling factors of 55.5% and 45.13% respectively. The simulation model is shown in Fig. 6(a) along with its equivalent circuit model in Fig. 6(b). Several simulations have been performed to study cross polarization in the case of the T-shaped cell, it has been demonstrated that the contribution of this component does not exist, or it is negligible.

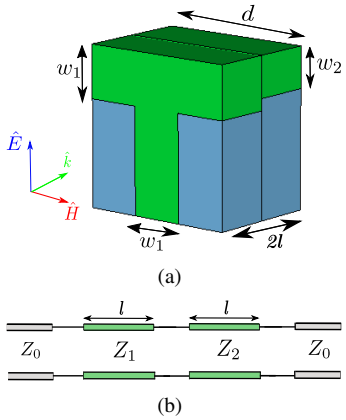

Fig. 6. Simulation setup to test the validity of the model (a) Two T-shape unit cells together; $d = 2.7\,\text{mm}$, $l = 1\,\text{mm}$, $w_1 = 0.9\,\text{mm}$, $w_2 = 0.7\,\text{mm}$ (b) Equivalent circuit of the two unit cells arranged, $Z_1 = 279.2\Omega, Z_2 = 293.5\Omega$.

In Fig. 7(a) - Fig. 7(d), we compute the S parameters of the two-layer structure under the incidence of a plane wave with the electric field polarized along y. The figures represent results obtained by CST and the equivalent circuit. We can see the excellent agreement between the models in the range of frequencies studied. These results allow us to willingly control the phase of the reflected and transmitted wave on the dielectric unit cell.

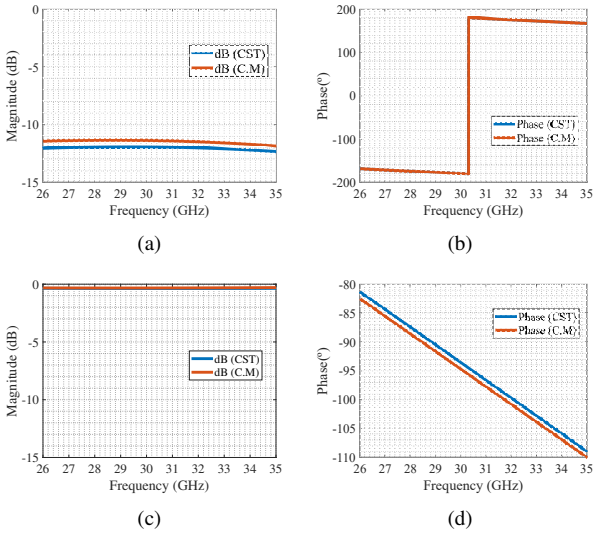

Fig. 7. Scattering parameters for the cascade of two T-shaped unit cells (a) Magnitude of the reflection coefficient in dB (b) Phase of the reflection coefficient. (c) Magnitude of the transmission coefficient in dB (d) Phase of the transmission coefficient. The range of frequency is chosen around $\lambda/2$ to show the most interesting results.

To further test our model, we have studied an arrangement of three consecutive unit cells. The simulations have been performed using two square-shaped unit cells and a T-shaped unit cell. The simulation model and its equivalent circuit model are displayed in Fig. 8(a). The used permittivities are $\varepsilon_r = 3, 6, 10$ for the first square-shaped unit cell, the T-shaped unit cell and the second square-shaped unit cell, respectively.

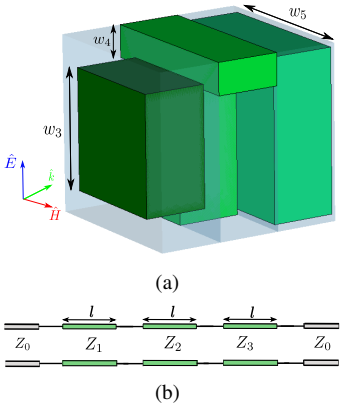

Fig. 8. Simulation setup to test the validity of the model (a) Three cells together: Square - T-shape - Square; $w_3 = 1.87\,\text{mm}$, $w_4 = 0.5\,\text{mm}$, $w_5 = 2.53\,\text{mm}$. $l = 1\,\text{mm}$ (b) Equivalent circuit of the three unit cells arranged, $Z_1 = 289.6\Omega, Z_2 = 252.7\Omega, Z_3 = 137.2\Omega$.

The filling factors associated with each of these unit cells are 48%, 33% and 88%, respectively.

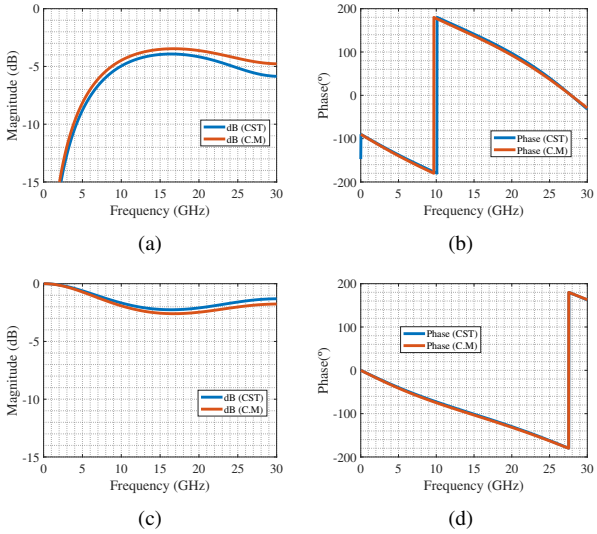

Fig. 9. Scattering parameters for the cascade of two square cells and T-shaped unit cells (a) Magnitude of the reflection coefficient in dB (b) Phase of the reflection coefficient. (c) Magnitude of the transmission coefficient in dB (d) Phase of the transmission coefficient. The range of frequency is chosen around $\lambda/2$ to show the most interesting results.

In Fig. 9(a) - Fig. 9(d), we compute the S parameters of the three-layer structure under the incidence of a vertically-polarized electric field. The circuit parameters have been obtained by computing the corresponding $\varepsilon_{\text{r, eff}}$ values thanks to the equations (3) and (4), and introducing them in (1) and (2) to get the propagation constant and the characteristic impedances of each transmission line section. We can see the excellent agreement between the models in the range of frequencies studied, using the semi-analytic equations to calculate the effective permittivity.

IV. Conclusion

This study is focused on the characterization of 3D fully-dielectric unit cells. Two dielectric unit cell designs have been analyzed. The geometries chosen for the dielectric cells have been a square and a T-shape. The extraction of the main parameters of the dielectric unit cell has been obtained by the ABCD matrix method. In addition, the modeling of the effective permittivity versus filling factor curves have been obtained for the dielectric unit cells where their electrical sizes are up to $\lambda/2$. Based on this characterization, the unit cells have been modeled by means of circuit models. These efficient models have been compared with full-wave simulated models of dielectric unit cell concatenations with different geometries. A good agreement is obtained between the simulated results and those given by the circuit models over the whole frequency range under study.

Acknowledgment

This work was supported in part by the Spanish Government under Project PID2020-112545RB-C54, Project RTI2018-102002-A-I00, Project TED2021-129938B-I00 and Project TED2021-131699B-I00; in part by the "Junta de Andalucía" under Project A-TIC-608-UGR20, Project PYC20-RE-012-UGR, and Project P18.RT.4830; in part by the Predoctoral Grant FPU18/01965; in part by the COST Action Symat (CA18223), supported by COST (European Cooperation in Science and Technology), and in part by a Leonardo Grant of the BBVA foundation. The authors acknowledge the support of the BBVA foundation for the funds associated to a project belonging to the program Leonardo Grants 2021 for researchers and cultural creators from the BBVA foundation. The BBVA Foundation accepts no responsibility for the opinions, statements and contents included in the project and/or the results thereof, which are entirely the responsibility of the authors

References

[1] M. H. Neshati and Z. Wu, "The determination of the resonance frequency of the $TE_{111}{}^{y}$ mode in a rectangular dielectric resonator for antenna application," in *2001 Eleventh International Conference on Antennas and Propagation, (IEE Conf. Publ. No. 480)*, 2001, pp. 53-56 vol.1.

[2] Y. -L. Li and K. -M. Luk, "A Low-Cost 3-D Printed THz Open Resonator Antenna," *IEEE Antennas Wirel. Propag. Lett.*, 2022, doi: 10.1109/LAWP.2022.3202927.

[3] Y. He, Z. Gao, D. Jia, W. Zhang, B. Du and Z. N. Chen, "Dielectric Metamaterial-Based Impedance-Matched Elements for Broadband Reflectarray," *IEEE Trans. Antennas Propag.*, vol. 65, no. 12, pp. 7019-7028, Dec. 2017.

[4] P. Mei, S. Zhang and G. F. Pedersen, "A Wideband 3-D Printed Reflectarray Antenna With Mechanically Reconfigurable Polarization," *IEEE Antennas Wirel. Propag. Lett.*, vol. 19, no. 10, pp. 1798-1802, Oct. 2020.

[5] A. Massaccesi *et al.*, "3D-Printable Dielectric Transmitarray With Enhanced Bandwidth at Millimeter-Waves," *IEE Access*, vol. 6, pp. 46407-46418, 2018.

[6] X. Liu *et al.*, "Ultrabroadband All-Dielectric Transmitarray Designing Based on Genetic Algorithm Optimization and 3-D Print Technology," *IEEE Trans. Antennas Propag.*, vol. 69, no. 4, pp. 2003-2012, April 2021.

[7] A. Petosa and A. Ittipiboon, "A fresnel lens designed using a perforated dielectric," in *2002 9th International Symposium on Antenna Technology and Applied Electromagnetics*, 2002, pp. 1-4.

[8] M. Imbert, A. Papió, F. De Flaviis, L. Jofre and J. Romeu, "Design and Performance Evaluation of a Dielectric Flat Lens Antenna for Millimeter-Wave Applications," *IEEE Antennas Wirel. Propag. Lett.*, vol. 14, pp. 342-345, 2015.

[9] S. Zhang, R. K. Arya, S. Pandey, Y. Vardaxoglou, W. Whittow, and R. Mittra, "3D-printed planar graded index lenses," *Microw., Antennas Propag.*, vol. 10, no. 13, pp. 1411–1419, Oct. 2016.

[10] S. Zhang, "Design and fabrication of 3D-printed planar Fresnel zone plate lens," *Electron. Lett.*, vol. 52, no. 10, pp. 833–835, May 2016.

[11] O. Bjorkqvist, O. Zetterstrom, and O. Quevedo-Teruel, "Additive manufactured dielectric Gutman lens," *Electron. Lett.*, vol. 55, no. 25, pp. 1318–1320, Dec. 2019.

[12] J. M. Monkevich and G. P. Le Sage, "Design and Fabrication of a Custom-Dielectric Fresnel Multi-Zone Plate Lens Antenna Using Additive Manufacturing Techniques," *IEEE Access*, vol. 7, pp. 61452-61460, 2019.

[13] Á. F. Vaquero, M. R. Pino, M. Arrebola, S. A. Matos, J. R. Costa and C. A. Fernandes, "Bessel Beam Generation Using Dielectric Planar Lenses at Millimeter Frequencies," *IEEE Access*, vol. 8, pp. 216185-216196, 2020.

[14] K. H. Jeong and N. Ghalichechian, "3D-printed 4-zone Ka-band Fresnel lens: Design, fabrication, and measurement," *Microw., Antennas Propag.*, vol. 14, no. 1, pp. 28–35, 2020.

[15] C. Wang, J. Wu and Y. -X. Guo, "A 3-D-Printed Wideband Circularly Polarized Parallel-Plate Luneburg Lens Antenna," *IEEE Trans. Antennas Propag.*, vol. 68, no. 6, pp. 4944-4949, June 2020.

[16] J. M. Poyanco, F. Pizarro, and E. Rajo-Iglesias, "Wideband hyperbolic flat lens in the ka-band based on 3d-printing and transformation optics," *Appl. Phys. Lett.*, vol. 118, no. 12, p. 123503, 2021.

[17] S. Lei, K. Han, X. Li and G. Wei, "A Design of Broadband 3-D-Printed Circularly Polarized Spherical Luneburg Lens Antenna for X-Band," *IEEE Antennas Wirel. Propag. Lett.*, vol. 20, no. 4, pp. 528-532, April 2021.

[18] S. Zhang, R. K. Arya, W. G. Whittow, D. Cadman, R. Mittra and J. C. Vardaxoglou, "Ultra-Wideband Flat Metamaterial GRIN Lenses Assisted With Additive Manufacturing Technique," *IEEE Trans. Antennas Propag.*, vol. 69, no. 7, pp. 3788-3799, July 2021.

[19] S. Moreno-Rodríguez, M. A. Balmaseda-Márquez, J. Carmona-Murillo and, Á. Palomares-Caballero, "Polarization-Insensitive Unit Cells for a Cost-Effective Design of a 3-D-Printed Fresnel-Lens Antenna" *Electronics*, vol. 11(3), no. 338, 2022.

[20] S. Zhang, P. Liu and W. Whittow, "Design and Fabrication of 3-D-Printed High-Gain Broadband Fresnel Zone Lens Using Hybrid Groove-Perforation Method for Millimeter-Wave Applications," *IEEE Antennas Wirel. Propag. Lett.*, vol. 21, no. 1, pp. 34-38, Jan. 2022.

[21] J. S. Colburn and Y. Rahmat-Samii, "Patch antennas on externally perforated high dielectric constant substrates," *IEEE Trans. Antennas Propag.*, vol. 47, no. 12, pp. 1785-1794, Dec. 1999.

[22] Pozar, David M. (2011) Microwave Engineering. 4th Edition. Wiley, New York.